Hindawi Publishing Corporation
International Journal of Photoenergy
Volume 2012, Article ID 528637, 8 pages
doi:10.1155/2012/528637

Research Article

Effects of Calcination Temperature on Preparation of Boron-Doped TiO_2 by Sol-Gel Method

Wenjie Zhang, Bo Yang, and Jinlei Chen

School of Environmental and Chemical Engineering, Shenyang Ligong University, Shenyang 110159, China

Correspondence should be addressed to Wenjie Zhang, metalzhang@yahoo.com.cn

Received 5 January 2012; Revised 5 February 2012; Accepted 6 February 2012

Academic Editor: Weifeng Yao

Boron-doped TiO_2 photocatalyst was prepared by a modified sol-gel method. Being calcinated at temperatures from 300°C to 600°C, all the 3% B-TiO_2 samples presented anatase TiO_2 phase, and TiO_2 crystallite sizes were calculated to be 7.6, 10.3, 13.6, and 27.3 nm, respectively. The samples were composed of irregular particles with rough surfaces in the size range within 3 μm. Ti atoms were in an octahedron skeleton and existed mainly in the form of Ti^{4+}, while the Ti-O-B structure was the main boron existing form in the 3% B-TiO_2 sample. When calcination temperature increased from 300°C to 600°C, specific surface area decreased sharply from 205.6 m^2/g to 31.8 m^2/g. The average pore diameter was 10.53 nm with accumulative pore volume of 0.244 mL/g for the 3% B-TiO_2 sample calcinated at 400°C, which performed optimal photocatalytic degradation activity. After 90 min of UV-light irradiation, degradation rate of methyl orange was 96.7% on the optimized photocatalyst.

1. Introduction

In recent years, many kinds of metal or nonmetal doped TiO_2 photocatalysts were prepared because semiconductive TiO_2 was considered to be the most attractive photocatalyst due to its properties of chemically stable, nontoxic, high efficient, and relatively inexpensive [1, 2]. TiO_2 has attracted much attention in view of its practical applications such as self-cleaning surfaces, wastewater and air purification, bacteria inactivation, and CO_2 photoconversion to methane and low hydrocarbons. Many environmental pollutants can be degraded by oxidation and reduction processes on TiO_2 surface [3–5]. However, the application of TiO_2 is limited by its UV activation requirement because of its large band gap (3.2 eV in the anatase phase), and recombination rate of photogenerated electrons and holes is usually very quickly.

Doping technology is one of the effective means to overcome the disadvantages of TiO_2. Since Asahi et al. [6] found out that N doped into TiO_2 effectively enhanced the photocatalytic activity of TiO_2, there has been an explosion of interest in TiO_2 doping with non-metal ions because of high thermal stability and low carrier recombination centers of nonmetals doped TiO_2 nanostructures. A variety of nonmetal ions such as N [7–9], C [10], S [11], F [12], P [13], I [14], and B [15, 16] has been explored to promote separation of photogenerated charges in TiO_2. Due to the electron deficiency structure of boron, boron-doped TiO_2 has already attracted much attention, and researches have increasingly focused on the development of boron doped TiO_2 systems in recent years. Zhao et al. [17] reported that doping with B can extend the spectrum response of TiO_2 to visible region and thus can improve its visible light photocatalytic activity. Chen et al. [18] found that B-doped TiO_2 showed higher photocatalytic activity than that of pure TiO_2 in photocatalytic NADH regeneration. They ascribed the improvement of photocatalytic activity to the formation of Ti^{3+}, which can facilitate the separation of photoexcited electrons and holes and slow their recombination rate. Yuan et al. [19] prepared B and N codoped TiO_2 photocatalyst via sol-gel method and found that interstitial N and [NOB] species in the TiO_2 crystal lattice narrowed band gap and extended optical absorption of TiO_2. Xu et al. [20] indicated that low-temperature hydrothermal method could be used to prepare boron-doped TiO_2, and the photocatalyst showed larger surface area and higher photocatalytic activity than that prepared by sol-gel method. Zaleska et al. [21] used a simple surface impregnation method to prepare

boron-modified TiO_2, and boron as a B-O-Ti species existed in the surface of TiO_2 grains.

Despite the work dedicated to the properties of photoactive B-TiO_2, most work focused on effects of B doping amounts. Very limited published works were related to the effects of calcination temperature on properties of B-doped TiO_2. In the present work, 3% boron-doped TiO_2-based photocatalysts were prepared by sol-gel method at different calcination temperatures using tributyl borate as boron precursor, and their characteristics were investigated by XRD, SEM, FT-IR, XPS, surface area (BET), and porosity determination (BJH). Photocatalytic degradation of an organic azo-dye, methyl orange, was investigated under ultraviolet irradiation. The effects of calcination temperature on structure, surface area, crystallinity, and photocatalytic activity of B-TiO_2 photocatalyst were systematically investigated.

2. Experimental

2.1. Preparation of B-TiO_2 Photocatalysts. 3 wt% boron-doped TiO_2 photocatalysts were prepared by a modified sol-gel approach. The detailed process was described as follows. Tetrabutyl titanate of chemical pure grade was chosen as the Ti precursor and tributyl borate (99.5%) was used as the boron source. Hydrochloric acid (HCl) and anhydrous ethanol were in the analytical reagent grade. 8 mL anhydrous ethanol and 0.1 mL hydrochloric acid were mixed in a beaker, and then 2 mL tetrabutyl titanate and desired volume of tributyl borate were dropwisely added to the former solution under constant magnetic stirring to prepare solution 1. Meanwhile, 1 mL of distilled water was mixed with 4 mL anhydrous ethanol to prepare solution 2. After solution 1 was stirred for 30 min, solution 2 was dropwisely added into solution 1. The final mixed solution was continuously stirred until the formation of a gel. After aging for 24 h at room temperature, the gel was dried at 80°C for 8 h. Subsequently, the obtained solid was grinded and calcinated at different temperatures for 3 h, respectively. The obtained 3% boron-doped TiO_2 was ascribed as 3% B-TiO_2 in the following experiments.

2.2. Catalyst Characterization. X-ray diffraction (XRD) patterns were obtained by a Rigaku D/Max-rB diffractometer using Cu Ka radiation. The XRD estimation of crystallite size was based on the Scherrer formula. Scanning electron microscopy (SEM, Hitachi, S-3400N) was used for morphology characterization of B-doped TiO_2 crystal. The samples for SEM imaging were coated with a thin layer of gold film to avoid charging. FT-IR spectra of the samples were obtained using a Fourier transform infrared (FT-IR) spectrometer (WQF-410) with KBr pellets. The samples were analyzed in the wavenumber range of 4000–400 cm^{-1}. The elemental composition of 3% B-TiO_2 nanocrytals was determined by X-ray photoelectron spectroscopy (XPS, MULTILAB2000). Specific surface area measurements were performed using a surface area and pore size analyzer (F-sorb 3400). The specific surface area was determined by the multipoint BET method using the adsorption data in the relative pressure (P/P_0) range of 0.05–0.25. The desorption isotherm was used to determine pore size distribution using the Barrett, Joyner, and Halenda (BJH) method.

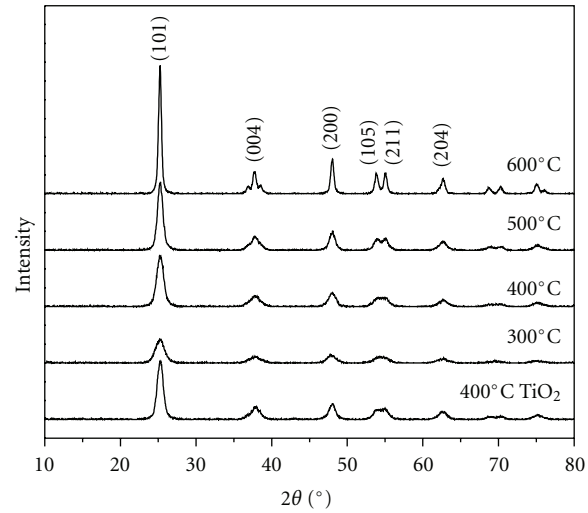

Figure 1: XRD patterns of 3% B-TiO_2 samples with different calcination temperatures and the pure TiO_2 calcinated at 400°C.

2.3. Measurement of Photocatalytic Activity. The effectiveness of B-doped TiO_2 nanocrystal was evaluated by degradation of methyl orange (MO) solution under UV light irradiation. Before photocatalytic experiment, adsorption of MO solution in the dark on the 3% B-TiO_2 photocatalyst was measured in the suspension. 50 mL of 10 mg/L methyl orange aqueous solution was mixed with 30 mg photocatalyst in a 250 mL beaker. The suspension was stirred magnetically for 20 min to reach adsorption equilibrium. After that, 5 mL suspension was taken out of the reactor and filtrated through a millipore filter (pore size 0.45 μm) to remove the photocatalyst. Finally, absorbency of the solution was measured using a 721E spectrophotometer at the MO maximum absorption wavelength of 468 nm.

Photocatalytic activities of the prepared catalysts were evaluated afterwards. A 20 W ultraviolet lamp was located over the 250 mL beaker with a distance of 11 cm from the lamp to the surface of the solution. The lamp can irradiate UV light at wavelength of 253.7 nm with the intensity of 1100 $\mu W/cm^2$. In prior to turn on the lamp, the solution should ensure adsorption equilibrium according to the above process. Irradiation time in the subsequent experiments was set for 30 min except for the prolonged time reaction. After photocatalytic reaction, 5 mL of the suspension was filtrated through millipore filter to measure the change of MO concentration.

3. Results and Discussion

3.1. Characterization of B-TiO_2 Photocatalysts. XRD was carried out to investigate phase structure of B-TiO_2. Figure 1 shows XRD patterns of 3% B-TiO_2 samples that were calcinated at 300, 400, 500, and 600°C for 3 h, respectively. All the diffraction peaks in the patterns well match the diffraction

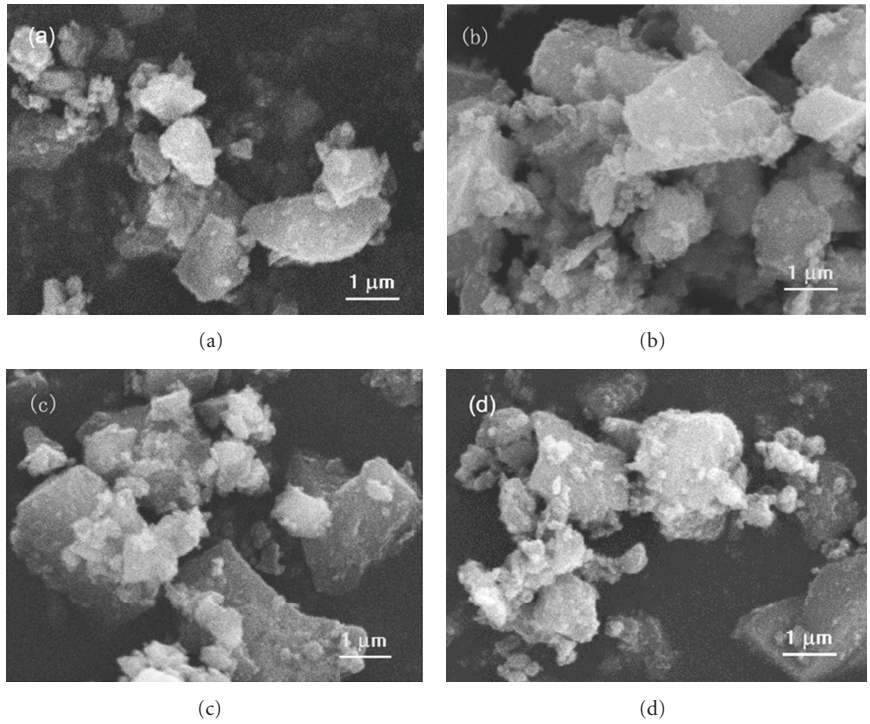

(a) (b) (c) (d)

Figure 2: SEM images of 3% B-TiO_2 samples calcinated at (a) 300°C, (b) 400°C, (c) 500°C, and (d) 600°C, respectively.

peaks of anatase TiO_2 crystallite. There are no peaks showing impurities such as B_2O_3 and TiB_2 or other TiO_2 phases like rutile and brookite existing in the samples. The XRD analysis can not confirm any formation of boron containing compound, probably because it is in the amorphous state in the photocatalysts. Grzmil et al. reported formation of B_2O_3 when boron-doped TiO_2 was calcinated at 1000°C [22]. It indicates that low calcination temperature might be the reason for formation of amorphous boron phase in the samples.

Being calcinated at temperatures from 300°C to 600°C, all the samples present anatase TiO_2 phase, and there is no peak demonstrating transformation from anatase TiO_2 to rutile TiO_2. Grzmil et al. [22] and Chen et al. [18] pointed out that boron-doped TiO_2 would undergo anatase-rutile transformation during calcination above 700°C. Therefore, the results confirm that no TiO_2 phase change occurred during calcination process at temperatures rising from 300°C to 600°C.

The TiO_2 crystallinity and crystallite size increased as calcination temperature increased based on the intensities of characteristic XRD peaks. The peak intensities of anatase TiO_2 phase become stronger, and the width of the peaks gets narrower for the samples calcinated at higher temperatures. It indicates that calcination can lead to TiO_2 crystal growth with increasing temperature. Crystallite sizes of the samples were calculated using the Scherrer formula according to Full Width at Half Maximum (FWHM) analysis of the anatase (101) plane diffraction peak. The crystallite sizes of B-TiO_2 prepared at calcination temperatures from 300°C to 600°C were calculated to be 7.6, 10.3, 13.6, and 27.3 nm, respectively, revealing an obvious crystallite growing under high-temperature calcination treatment.

Surface morphology is quite essential for photocatalytic activity of the materials. Figures 2(a) to 2(d) show boron-doped TiO_2 samples calcinated at 300, 400, 500, and 600°C. The prepared samples are composed of irregular particles with fairly rough surfaces in the size range within 3 μm. The small particles among the big ones came from grinding after calcination. The particle size seems quite suitable for suspending in methyl orange solution under magnetic stirring. There was no strong particles aggregation during sol-gel preparation and calcination processes. All of the 3% B-TiO_2 samples can undergo well dispersion without apparent deposition during photocatalytic reaction.

Figure 3 shows FT-IR spectra of 3% B-TiO_2 samples with different calcination temperature. For all samples, the bands at 3384 cm^{-1} and 1621 cm^{-1} are assigned to the stretching of hydroxyl groups and the bending vibration of H_2O adsorbed on the surface of the samples. There are peaks at 469 cm^{-1} and 670 cm^{-1} for the stretching of Ti–O bond and the bending vibration of Ti–O bond, respectively. In the IR spectra of the samples, another peak appears at 1397 cm^{-1} can be ascribed to the vibration of tri-coordinated boron [23]. Furthermore, neither absorption peak corresponding to pure B_2O_3 (1202 cm^{-1}) [22] nor peak of incorporated BO_4 (1096 cm^{-1}) [24] appears in the spectra. It reveals that boron is introduced into the titania framework in the form of B-O-Ti bond, and this structure is further confirmed by XPS measurements later. However, the peak at 1397 cm^{-1} [23, 25] corresponding to tricoordinated boron is weakened after high-temperature calcination, indicating that

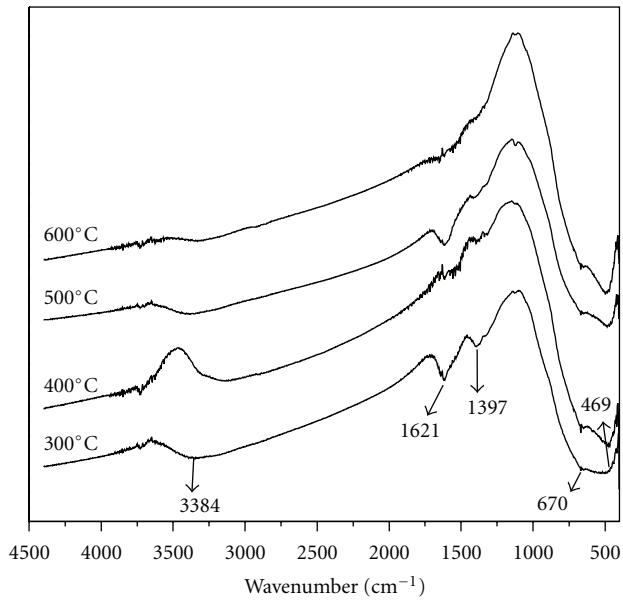

Figure 3: FT-IR spectra of 3% B-TiO_2 samples with different calcination temperature.

boron in Ti-O-B form preferably appears at low temperature calcination.

Figure 4(a) shows XPS B1*s* spectrum of 3% boron-doped TiO_2 photocatalyst prepared by sol-gel method followed by calcination at 400°C. Normally, B1*s* electron-binding energy peak situates around 188 eV–194 eV for B-TiO_2. In the figure, B1*s* peak can be separated to three independent peaks using XPSPEAK 4.1 software. This means that different chemical forms of B atoms might exist in B-doped TiO_2 nanoparticles. The standard binding energy of B1*s* in B_2O_3 or H_3BO_3 equals to 193.0 eV (B–O bond) and in TiB_2 equals to 187.5 eV (B–Ti bond) [18]. In the figure, the first peak at 192.9 eV is related to B–O–B bonds in B_2O_3 or H_3BO_3 and the low energy peak at 189.6 eV corresponds to boron incorporated into the TiO_2 lattice through occupying O sites to form O-Ti-B band. Su et al. also pointed out that the peak at 189.6 eV might correspond to B-Ti in TiB_2 [26]. The strongest peak at 191.7 eV is related to boron that is probably weaved into the interstitial TiO_2 and exists in the form of Ti-O-B structure [23, 27, 28]. The Ti-O-B structure is the main boron existing form in the 3% B-TiO_2 sample.

Figure 4(b) shows XPS Ti2*p* spectra of 3% B-TiO_2. There are two isolated symmetrical peaks in the XPS patterns, showing that Ti atoms are in an octahedron skeleton and existed mainly in the form of Ti^{4+}. The binding energies of Ti2*p*3/2 and Ti2*p*1/2 for 3% B-TiO_2 sample are at 456.6 eV and 462.2 eV, and distance between Ti2*p*3/2 and Ti2*p*1/2 peaks is 5.6 eV (The standard value is 5.6 to 5.7 eV [29]). It was reported that boron doping favored the formation of Ti^{3+} on the surface of TiO_2 [30, 31], but there is no evidence of Ti^{3+} formation in Figure 4(b).

As shown in Figure 4(c), XPS O1*s* region is composed of three peaks situating at 532.7 eV, 531.7 eV, and 530.2 eV. The first peak at 532.7 eV is related to oxygen in the TiO_2 crystal lattice, and the second peak at 531.7 eV corresponds to the surface hydroxyl groups. The peak at 530.2 eV indicates oxygen in the Ti–O–B bond [21], which is in accordance to the result of XPS B1*s* region. Therefore, XPS analysis confirms that sol-gel synthesis allows incorporation of boron atoms into TiO_2 matrix. Figure 4(d) shows XPS C1*s* spectrum of the 3% B-TiO_2 sample. The peak at lower binding energy of 284.8 eV was used for calibration of the XPS results, and the peak at 289.3 eV is attributed to the adsorbed carbon on the sample.

Table 1: Lattice parameters and BET surface areas of 3% B-TiO_2 samples calcinated at different temperatures.

Calcination temperature /°C	Surface area /m^2/g	a(=b) /10^{-1} nm	c /10^{-1} nm	V /10^{-3} nm^3
300	205.6	3.7852	9.4642	135.6005
400	127.8	3.7997	9.5008	136.2833
500	88.6	3.7901	9.5532	137.2303
600	31.8	3.7985	9.5678	138.0499

In order to study porous status of the boron-doped TiO_2 materials, Brunauer-Emmett-Teller nitrogen sorption measurements were carried out. N_2 molecules were in single or multiple layers adsorbed on the internal pore surface of the materials. As shown in Figure 5(a), N_2 desorption changed significantly at relative pressure between 0.95 and 0.6 in N_2 desorption process, which was mainly caused by capillary aggregation of N_2 molecules occurring in micropores inside the material [32]. Figure 5(b) shows that pore size of 3% B-TiO_2 mainly distributes in the range from 1.5 nm to 18 nm. The average pore diameter of 3% B-TiO_2 calcinated at 400°C is 10.53 nm, and the accumulative pore volume is 0.244 mL/g for the material.

As shown in Table 1, the specific surface areas of 3% B-TiO_2 samples decreased continuously with increasing calcination temperature. When calcination temperature increased from 300°C to 600°C, surface area decreased sharply from 205.6 m^2/g to 31.8 m^2/g. The sample calcinated at 300°C had the largest surface area because organic substances did not burn out totally at low temperature, and the residual carbon contributed to the large BET surface area. Lattice parameters were obtained by using Bragg's law ($2d \sin\theta = \lambda$) and a formula for a tetragonal system, $1/d^2 = (h^2 + k^2)/a^2 + l^2/c^2$. As summarized in Table 1, the lattice parameters of all the B-TiO_2 samples changed along with the change of calcination temperature. The cell volumes of 3% B-TiO_2 samples became larger at higher calcination temperature due to accelerated crystal growth at high temperature. It can also be deduced that crystallite sizes of B-TiO_2 could grow up with the increase of calcination temperature, which is confirmed by XRD analysis.

3.2. Photocatalytic Activity of 3% B-TiO_2. Photocatalytic activity of B-doped TiO_2 was evaluated by photocatalytic degradation of methyl orange under UV light irradiation. 3% B-TiO_2 prepared at different calcination temperature performed obviously different photocatalytic degradation

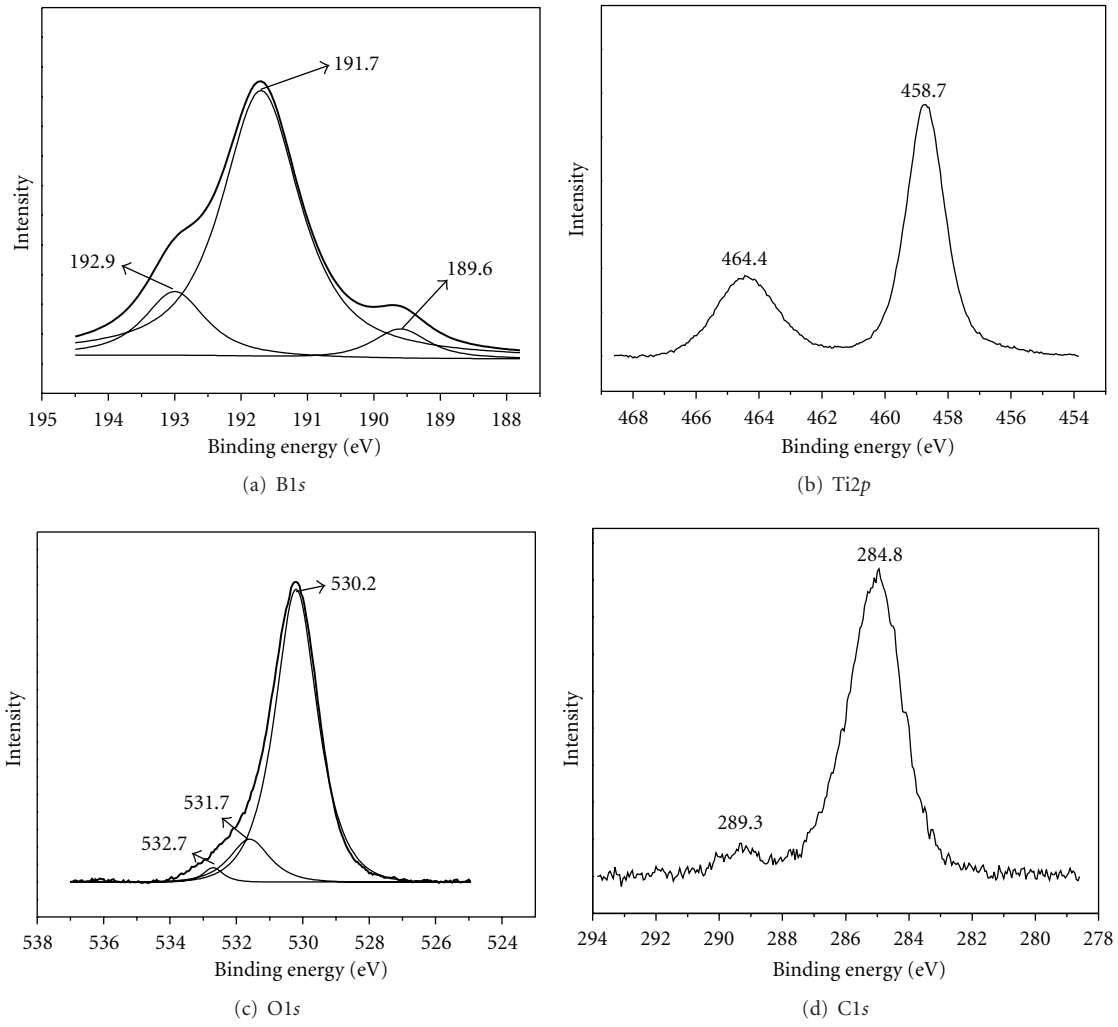

Figure 4: XPS patterns of 3% B-TiO_2 sample calcinated at 400°C.

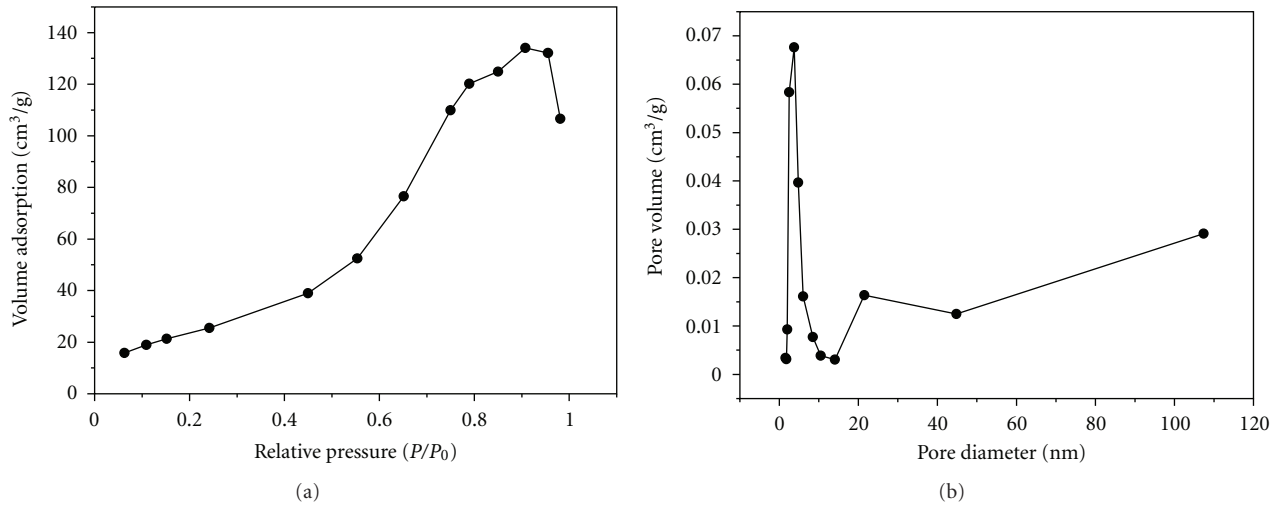

Figure 5: (a) N_2 desorption isotherms and (b) BJH pore size distribution of 3% B-TiO_2 samples calcinated at 400°C.

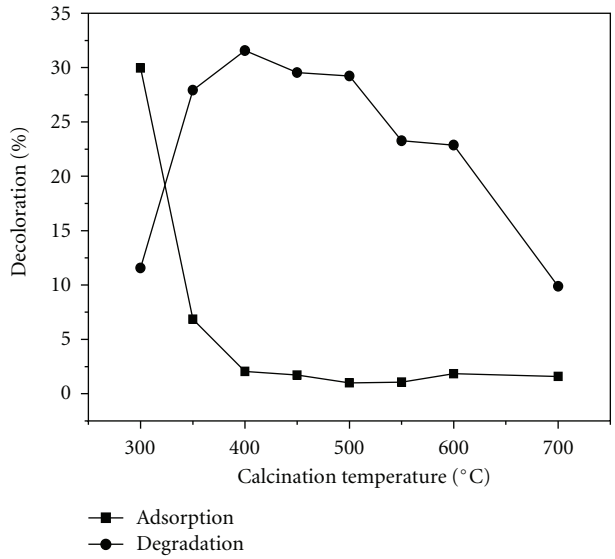

Figure 6: Photocatalytic activities of 3% B-TiO_2 samples calcinated at different temperatures.

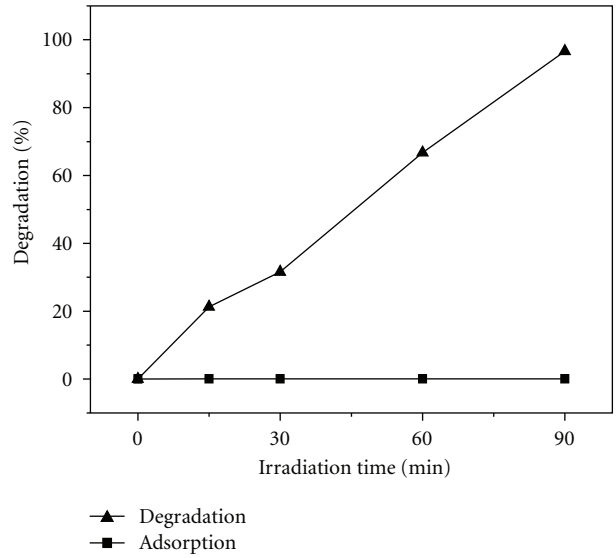

Figure 7: Photocatalytic activity of 3% B-TiO_2 sample with prolonged irradiation time.

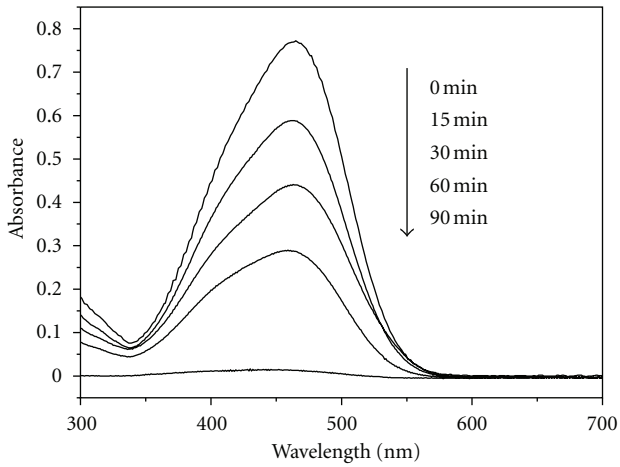

Figure 8: Absorption spectra of methyl orange solution during irradiation in the presence of 3% B-TiO_2.

activity, as shown in Figure 6. The optimal degradation rate was 31.5% on 3% B-TiO_2 sample calcinated at 400°C. The highest absorption of the dye was observed on 3% B-TiO_2 calcinated at 300°C. As previously indicated (see in Table 1), BET surface area of 3% B-TiO_2 calcinated at 300°C is 205.6 m^2/g, which is much more than that prepared at higher temperatures. Since 300°C was a low calcination temperature, some organic substances did not burn out totally, so that carbon residues caused the large BET surface area and high-absorption capacity. Low calcination temperature can be also responsible for insufficient formation of anatase TiO_2 crystals as the reason of low photocatalytic activity.

As can be seen from Figure 6, the adsorption of methyl orange changed slightly on the samples when calcination temperature varied from 400°C to 600°C, indicating thoroughly burning of organic substances at high temperatures. The sample that was calcinated at 400°C presented the optimal photocatalytic degradation activity. As described before, BET surface areas of the samples calcinated at 500°C and 600°C are smaller than that of the sample calcinated at 400°C. Meanwhile, FT-IR results show that the formation of Ti-O-B is weakened with the increase of calcination temperature. It can be deduced that the sample calcinated at 400°C represents the optimal physic-chemical and structural characteristics that are suitable for photocatalytic degradation of methyl orange.

Figure 7 presents the adsorption and photocatalytic activities of 3% B-TiO_2 calcinated at 400°C with prolonged irradiation time. Adsorption rate did not change noticeably after the dye reached its adsorption equilibrium. After 90 min of UV-light irradiation, degradation rate of methyl orange was 96.7% on 3% B-TiO_2 powder. It indicates that 3% B-TiO_2 has satisfactory photocatalytic activity.

Figure 8 shows absorption spectra of methyl orange aqueous solution in presence of 3% B-TiO_2 calcinated at 400°C. The maximum MO absorption peak at 468 nm gradually decreased during irradiation process. After 90 min of irradiation, the dye was completely decomposed according to disappearance of the main absorption peak, due to breaking up of methyl orange molecules into small parts under photocatalytic degradation.

4. Conclusion

Boron-doped TiO_2 photocatalyst was prepared by a modified sol-gel method. Crystallite sizes of boron-doped TiO_2 increased gradually, and BET surface areas of the 3% B-TiO_2 samples decreased sharply with increasing calcination temperature. Calcination temperature had no apparent impact on surface morphology of B-TiO_2. XPS and FT-IR results proved that the B-O-Ti structure in 3% B-TiO_2

reduced at high calcination temperature. The sample with the optimal photocatalytic activity was obtained after being calcinated at 400°C. Degradation rate of methyl orange was 96.7% after 90 minutes of UV irradiation.

Acknowledgments

This work was supported by the National Natural Science Foundation of China (no. 41071161 and 41130524), National Key Basic Research Foundation of China (2011CB403202), and Liaoning Science and Technology Project (2010229002).

References

[1] A. Fujishima and K. Honda, "Electrochemical photolysis of water at a semiconductor electrode," *Nature*, vol. 238, no. 5358, pp. 37–38, 1972.

[2] H. B. Li, G. C. Liu, S. G. Chen, and Q. C. Liu, "Novel Fe doped mesoporous TiO_2 microspheres: ultrasonic-hydrothermal synthesis, characterization, and photocatalytic properties," *Physica E*, vol. 42, no. 6, pp. 1844–1849, 2010.

[3] N. Sasirekha, S. J. S. Basha, and K. Shanthi, "Photocatalytic performance of Ru doped anatase mounted on silica for reduction of carbon dioxide," *Applied Catalysis B*, vol. 62, no. 1-2, pp. 169–180, 2006.

[4] G. H. Li, S. Ciston, Z. V. Saponjic et al., "Synthesizing mixed-phase TiO_2 nanocomposites using a hydrothermal method for photo-oxidation and photoreduction applications," *Journal of Catalysis*, vol. 253, no. 1, pp. 105–110, 2008.

[5] S. Guo, Z. B. Wu, H. Q. Wang, and F. Dong, "Synthesis of mesoporous TiO_2 nanorods via a mild template-free sono-chemical route and their photocatalytic performances," *Catalysis Communications*, vol. 10, no. 13, pp. 1766–1770, 2009.

[6] R. Asahi, T. Morikawa, T. Ohwaki, K. Aoki, and Y. Taga, "Visible-light photocatalysis in nitrogen-doped titanium oxides," *Science*, vol. 293, no. 5528, pp. 269–271, 2001.

[7] Q. Shen, W. Zhang, Z. P. Hao, and L. D. Zou, "A study on the synergistic adsorptive and photocatalytic activities of $TiO_{2-x}N_x$/Beta composite catalysts under visible light irradiation," *Chemical Engineering Journal*, vol. 165, no. 1, pp. 301–309, 2010.

[8] M. Qiao, S. S. Wu, Q. Chen, and J. Shen, "Novel trieth-anolamine assisted sol-gel synthesis of N-doped TiO_2 hollow spheres," *Materials Letters*, vol. 64, no. 12, pp. 1398–1400, 2010.

[9] J. Senthilnathan and L. Philip, "Photodegradation of methyl parathion and dichlorvos from drinking water with N-doped TiO_2 under solar radiation," *Chemical Engineering Journal*, vol. 172, pp. 678–688, 2011.

[10] Y. Li, M. Y. Ma, X. H. Wang, and X. H. Wang, "Inactivated properties of activated carbon-supported TiO_2 nanoparticles for bacteria and kinetic study," *Journal of Environmental Sciences*, vol. 20, no. 12, pp. 1527–1533, 2008.

[11] H. Tian, J. F. Ma, K. Li, and J. J. Li, "Hydrothermal synthesis of S-doped TiO_2 nanoparticles and their photocatalytic ability for degradation of methyl orange," *Ceramics International*, vol. 35, no. 3, pp. 1289–1292, 2009.

[12] J. J. Xu, Y. H. Ao, D. F. Fu, and C. W. Yuan, "Low-temperature preparation of F-doped TiO_2 film and its photocatalytic activity under solar light," *Applied Surface Science*, vol. 254, no. 10, pp. 3033–3038, 2008.

[13] Y. Y. Lv, L. S. Yu, H. Y. Huang, H. L. Liu, and Y. Y. Feng, "Preparation, characterization of P-doped TiO_2 nanoparticles and their excellent photocatalystic properties under the solar light irradiation," *Journal of Alloys and Compounds*, vol. 488, no. 1, pp. 314–319, 2009.

[14] Y. Ma, J. W. Fu, X. Tao, X. Li, and J. F. Chen, "Low temperature synthesis of iodine-doped TiO_2 nanocrystallites with enhanced visible-induced photocatalytic activity," *Applied Surface Science*, vol. 257, no. 11, pp. 5046–5051, 2011.

[15] R. Khan, S. W. Kim, T. J. Kim, and C. M. Nam, "Comparative study of the photocatalytic performance of boron-iron Co-doped and boron-doped TiO_2 nanoparticles," *Materials Chemistry and Physics*, vol. 112, no. 1, pp. 167–172, 2008.

[16] N. Lu, H. M. Zhao, J. Y. Li, X. Quan, and S. Chen, "Characterization of boron-doped TiO_2 nanotube arrays prepared by electrochemical method and its visible light activity," *Separation and Purification Technology*, vol. 62, no. 3, pp. 668–673, 2008.

[17] W. Zhao, W. H. Ma, C. H. Chen, J. C. Zhao, and Z. G. Shuai, "Efficient degradation of toxic organic pollutants with $Ni_2O_3/TiO_{2-x}B_x$ under visible irradiation," *Journal of the American Chemical Society*, vol. 126, no. 15, pp. 4782–4783, 2004.

[18] D. M. Chen, D. Yang, Q. Wang, and Z. Y. Jiang, "Effects of boron doping on photocatalytic activity and microstructure of titanium dioxide nanoparticles," *Industrial and Engineering Chemistry Research*, vol. 45, no. 12, pp. 4110–4116, 2006.

[19] J. Yuan, E. Wang, Y. Chen, W. Yang, J. Yao, and Y. Cao, "Doping mode, band structure and photocatalytic mechanism of B–N-codoped TiO_2," *Applied Surface Science*, vol. 257, no. 16, pp. 7335–7342, 2011.

[20] J. J. Xu, Y. H. Ao, M. D. Chen, and D. G. Fu, "Low-temperature preparation of boron-doped titania by hydrothermal method and its photocatalytic activity," *Journal of Alloys and Compounds*, vol. 484, no. 1-2, pp. 73–79, 2009.

[21] A. Zaleska, E. Grabowska, J. W. Sobczak, M. Gazda, and J. Hupka, "Photocatalytic activity of boron-modified TiO_2 under visible light: the effect of boron content, calcination temperature and TiO_2 matrix," *Applied Catalysis B*, vol. 89, no. 3-4, pp. 469–475, 2009.

[22] B. Grzmil, M. Gleń, B. Kic, and K. Lubkowski, "Preparation and characterization of single-modified TiO_2 for pigmentary applications," *Industrial and Engineering Chemistry Research*, vol. 50, no. 11, pp. 6535–6542, 2011.

[23] N. Feng, A. M. Zheng, Q. Wang et al., "Boron environments in B-doped and (B, N)-codoped TiO_2 photocatalysts: a combined solid-state NMR and theoretical calculation study," *The Journal of Physical Chemistry C*, vol. 115, no. 6, pp. 2709–2719, 2011.

[24] S. C. Moon, H. Mametsuka, E. Suzuki, and Y. Nakahara, "Characterization of titanium-boron binary oxides and their photocatalytic activity for stoichiometric decomposition of water," *Catalysis Today*, vol. 45, no. 1–4, pp. 79–84, 1998.

[25] H. L. Fei, Y. P. Liu, Y. P. Li et al., "Selective synthesis of borated meso-macroporous and mesoporous spherical TiO_2 with high photocatalytic activity," *Microporous and Mesoporous Materials*, vol. 102, no. 1–3, pp. 318–324, 2007.

[26] Y. L. Su, X. W. Zhang, S. Han, X. Q. Chen, and L. C. Lei, "F-B-codoping of anodized TiO_2 nanotubes using chemical vapor deposition," *Electrochemistry Communications*, vol. 9, no. 9, pp. 2291–2298, 2007.

[27] E. Finazzi, C. D. Valentin, and G. Pacchioni, "Nature of ti interstitials in reduced bulk anatase and rutile TiO_2," *Journal of Physical Chemistry C*, vol. 113, no. 9, pp. 3382–3385, 2009.

[28] X. N. Lu, B. Z. Tian, F. Chen, and J. L. Zhang, "Preparation of boron-doped TiO_2 films by autoclaved-sol method at low temperature and study on their photocatalytic activity," *Thin Solid Films*, vol. 519, no. 1, pp. 111–116, 2010.

[29] X. Q. Chen, X. W. Zhang, and L. C. Lei, "Electronic structures and photocatalysis properties under visible irradiation of F-doped TiO_2 nanotube arrays," *Journal of Inorganic Materials*, vol. 26, no. 4, pp. 369–374, 2011.

[30] M. Fittipaldi, V. Gombac, T. Montini, P. Fornasiero, and M. Graziani, "A high-frequency (95 GHz) electron paramagnetic resonance study of B-doped TiO_2 photocatalysts," *Inorganica Chimica Acta*, vol. 361, no. 14-15, pp. 3980–3987, 2008.

[31] Y. M. Wu, M. Y. Xing, J. L. Zhang, and F. Chen, "Effective visible light-active boron and carbon modified TiO_2 photocatalyst for degradation of organic pollutant," *Applied Catalysis B*, vol. 97, no. 1-2, pp. 182–189, 2010.

[32] J. Yuan, Y. K. Lv, Y. Li, and J. P. Li, "Preparation of mesoporous magnetic photocatalyst and its catalytic activity for degradation of nitrobenzene," *Chinese Journal of Catalysis*, vol. 31, no. 5, pp. 597–603, 2010.